Effect of the cold Nazca Slab on the depth of the 660 km discontinuity in South America

Marcelo Belentani Bianchi [a], Marcelo Assumpção [a,*], Clinton Koch [b], Susan Beck [b]

[a] *University of São Paulo, Institute of Astronomy, Geophysics and Atmospheric Sciences, Brazil*
[b] *University of Arizona, Department of Geosciences, USA*

A B S T R A C T

The Nazca plate subducting beneath South America makes the 660 km discontinuity deeper and the mantle transition zone (MTZ) thicker under the continent. MTZ variations are often associated with mantle temperature and, therefore, can help confirm the slab position at greater depths. Recent P- and S-wave tomography results show the Nazca plate, near 20° S, being held below the MTZ for longitudes between 70° W and 55° W. We used 63,809 P-wave receiver functions from 1216 stations (using the LQT components of the incident ray system) to image the MTZ in South America. The receiver functions were corrected for move-out, stacked in cells of 3° x 3° degrees every 1° x 1°. We obtained 54,389 RF traces imaging the 410 km and the 660 km discontinuities. The discontinuity times were corrected using the SL2013 global tomography model to obtain depths. A thickened MTZ follows the trend of the Nazca plate beneath the sub-Andes. To the north of 18°S the thickened MTZ is only about 250 km wide; to the south, the thickened zone reaches up to a 1100 km width. This observation clearly indicates that the Nazca slab flattens close to the 660 km discontinuity lowering the mantle temperature and thickening the MTZ. The 660 km discontinuity is more affected than the 410 km, which is consistent with the Nazca slab being held just below the MTZ and not inside the MTZ in most of the region.

1. Introduction

Since the 1990's depths to the 410 and 660 km seismic discontinuities in the mantle have been mapped using both receiver functions and SS precursors (e.g., Petersen et al., 1993; Shearer and Masters, 1992) looking for possible effects of temperature variations and mantle convection. More recent global and regional mappings (such as Lawrence and Shearer, 2006; Braunmiller et al., 2006; Schmerr and Garnero, 2007; Huang et al., 2019) have been used to check effects of composition and water content. These major seismic discontinuities are due to high-pressure mineral phase changes: the 410 discontinuity is caused by transition from olivine (α) to wadsleyite (β spinel), and the 660 discontinuity is due to transitions from ringwoodite (γ spinel) to a mixture of silicate perovskite and magnesiowüstite (e.g., Bina and Helffrich, 2014). These two major discontinuities define the so called "mantle transition zone" (MTZ).

Temperature affects the two phase transitions in different ways: lower temperature makes the 410 km shallower and the 660 km deeper. These properties of the 410- and 660-km discontinuities make them suitable to study temperature variations in the mantle, either due to cold descending slabs or hot upwelling mantle material. The MTZ thickness (difference between the 660- and 410-km discontinuities) is often used as a way of checking temperature variations. Worldwide mappings of the MTZ show a general trend of thicker transition zone (shallower 410 and deeper 660) in regions dominated by subduction zones such as the west coast of South America (Lawrence and Shearer, 2006; Braunmiller et al., 2006; Huang et al., 2019), where the colder Nazca slab increases the MTZ thickness by ~10–20 km. A trend of thinner transition zone thickness is generally observed beneath mid-ocean ridges (e.g., Huang et al., 2019). For example, in the Tonga subduction zone Gilbert et al. (2001) found good correlation of the MTZ thickness with temperature variations inferred from seismic velocity anomalies. Similarly, beneath hot-spots Li et al. (2003) found usually thinner transition zone thickness (smaller time difference of the P-to-s conversions) than expected from the IASP91 global model.

In addition to temperature, water content also affects the width and depth of the discontinuities, especially the 410 (Wood, 1995; Litasov et al., 2006). Water may broaden the 410 transition by a few km and make it shallower. For example, a 2 wt % water content can raise the 410 km by 30 km (Smyth and Jacobsen, 2006). Receiver function studies in the Central Andes by Braunmiller et al. (2006) showed the 410 km elevated by ~34 km beneath La Paz station, which could be interpreted as a ~300 K cooler slab or a mantle saturated with water at 1 wt %. Water can also cause a depression of the 660 discontinuity by 10–15 km (Litasov et al., 2006; Smyth and Jacobsen, 2006).

Few regional studies of the mantle transition zone have been carried

---

* Corresponding author.
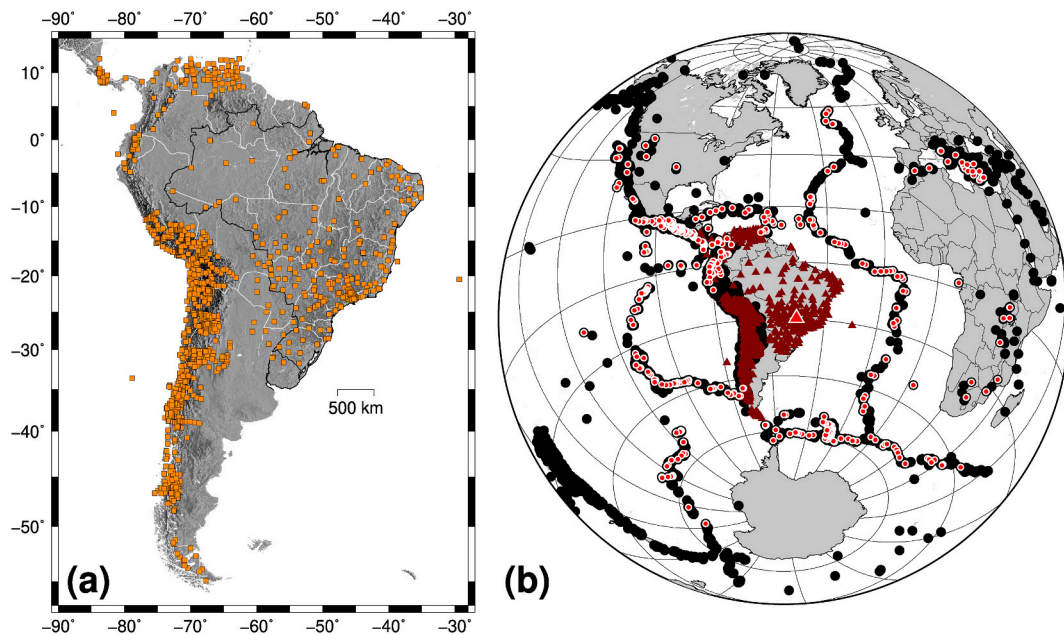 *E-mail address:* marcelo.assumpcao@iag.usp.br (M. Assumpção).

Fig. 1. Stations and events used for the Receiver Function processing. a) stations in South America from both permanent, open stations and temporary deployments accessed at IRIS. In Brazil we used stations of the open, permanent RSBR network (Bianchi et al., 2018) as well as the on-going temporary deployment of the "3-Basins Project" (2017–2020). (b) events used in this study. Black circles are all events searched for (magnitudes ≥5.0; distance range 30°–95° from any individual station), red circles are the selected events with receiver functions calculated for station BL.ITRB (red triangle). In total ~4800 events were used to yield 97,158 receiver functions.

out in mid-plate South America with receiver functions. Liu et al. (2003) did not detect any perturbation in the thickness of the mantle transition zone beneath the stable platform of SE Brazil and discarded high temperature as an explanation for the low-velocity "fossil plume" hypothesized by VanDecar et al. (1995). In Northeast Brazil, Pinheiro and Julià (2014) did not detect any topography in the mantle transition zone ruling out plume effects to explain intraplate Cenozoic magmatism in NE Brazil. More recently, Coelho (2019) showed that the Parnaíba intracratonic basin, NE Brazil, also has normal depths for the 410 and 660 discontinuities.

The Nazca slab in the northern part of South America crosses the MTZ and plunges into the lower mantle, as shown by global tomography models (Simmons et al., 2012; Fukao and Obayashi, 2013; Schaeffer and Lebedev, 2013; Hosseini et al., 2020) as well as by regional models (Portner et al., 2020; Rodríguez et al., 2021; Ciardelli et al., 2021). However, south of about 20°S, the geometry of the slab is not well defined yet. Some global models have shown the deep Nazca slab stagnant just above the 660 km discontinuity (Simmons et al., 2012; Fukao and Obayashi, 2013) whereas other models show the slab crossing directly the 660 km discontinuity (Celli et al., 2020; Hosseini et al., 2020). Regional, continental scale tomography inversions using teleseismic P and S waves (Scire et al., 2017; Portner et al., 2020; Rodríguez et al., 2021) have mapped the slab stagnant just below the transition zone, roughly between 700 and 1000 km depth. Whether the stagnant Nazca slab is within or below the transition zone has implications on mantle convection and composition. For example, stagnant slabs below the transition zone may imply higher density phases and layering in the lower mantle (Ballmer et al., 2015).

Here we use an extensive data set comprised of teleseismic P-wave data recorded by permanent stations in South America as well as by several temporary deployments, especially in the Andes and in Brazil.

We find that the depths of the 660 km discontinuity are lower than average over a wide region in South America which we attribute to lower temperatures due to a stagnant Nazca slab just beneath the mantle transition zone.

2. Database and processing

We compiled a data set comprised of all open, permanent broadband stations in South America as well as broadband temporary deployments, mainly in the Andes, available at the IRIS and GEOFON repository (Fig. 1a). For Brazil, we used a) open data from the Brazilian Seismographic Network (Bianchi et al., 2018), open data from previous temporary deployments, such as the BLSP2002 project (Feng et al., 2007) also available at IRIS, and c) data from the present temporary deployment in and around the Pantanal basin centered in West-Central Brazil, the FAPESP funded "3-Basins Project" (Rivadeneyra et al., 2019; Rocha et al., 2019). A total of 1216 stations were used.

Events above magnitude 5.0 were searched for in the distance range 30° to 90° from any station (Fig. 1b). A total of ~4800 events were selected to produce 97,158 receiver functions. The pre-processing steps consisted of: a) selection of events with a signal to noise ratio (SNR) > 2 for the vertical and horizontal components in the frequency band 0.7–2.5 Hz (which helps to discard noisy traces and malfunctioning channels); b) rotation from the ZNE to the LQT system (Fig. 2a); c) highpass filter at 1/40s, order 3; d) deconvolution of Q/L using an inversion filter with half the length of the signal window and a regularization value of 1 during filter determination; e) each individual trace was moved-out to a common slowness of 6.4 s/degree using the IASP91 model while its piercing point for 410 and 660 km discontinuities were computed. Fig. 2b shows the map with the piercing points for the 410 and 660 km discontinuities. During this pre-processing, receiver
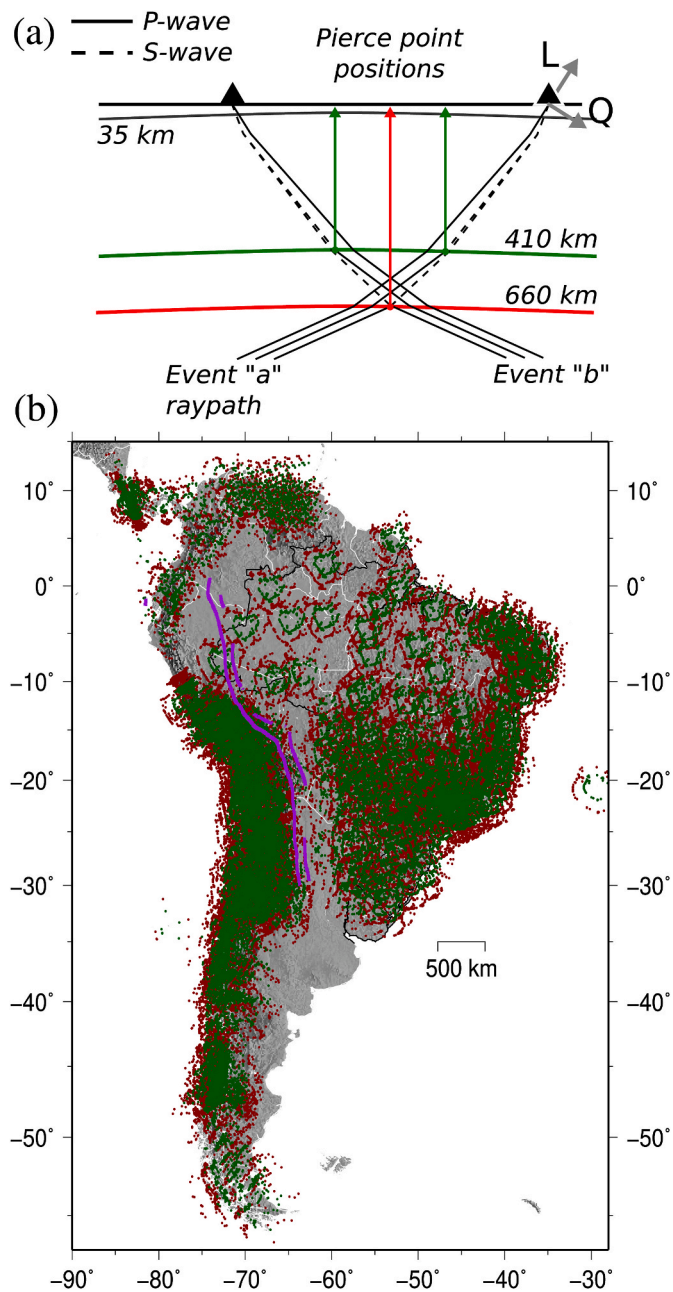
Fig. 2. Ps conversion ("piercing") points. a) Sketch of the "L, Q″ components and definition of the piercing points. Black triangles denote seismic stations. Solid and dashed rays are P- and S-wave paths. The piercing points are the P to S conversion points at each discontinuity. b) Map of all piercing points used in the study. Green dots are 410 km and red dots are 660 km piercing points. The piercing points are, on average, about 110 km and 225 km away from the station for the 410 km and 660 km discontinuities, respectively. The two purple lines are the 400 km and 600 km depth Benioff zone (Slab1.0 model, Hayes et al., 2012).

functions were low-pass filtered (for periods longer than 6s) using a 3rd order Butterworth filter to enhance the discontinuity conversions. The final data set had receiver function traces for event magnitudes in the range 5.5–8.3.

Move-out corrected and filtered receiver functions (RFs) were

stacked for all traces with piercing points within 3° x 3° windows. The windows were moved every 1° producing stacked RF traces spanning most of the continent (Fig. 3). The stacked traces were picked for the Ps conversion yielding Ps410 and Ps660 times, as shown in the seismic sections of Fig. 3. The initial picking was done automatically searching for the largest peak close to the expected arrival time of 44.1s and 68.1s, according to the IASP91 model for a slowness of 6.4 s/deg. All traces were then visually examined, using E-W profiles. Sometimes the automatic pick misses the correct peak (cycle-skipping); this was manually corrected by comparing with neighboring stacks and avoiding large steps in the travel time curve. This manual correction was applied to 4.5% of the traces for the 410 km, and 4.9% for the 660 km discontinuities. In addition, 2.5% of the automatic picks were discarded due to very low SNR. All picks are shown in Figs. S1 and S2 of the Supplementary material. No major oscillations of the 410 km Ps times are observed. On the other hand, a clear increase in the Ps times for the 660 km can be seen in some E-W cross sections, especially between 21°S and 24°S. The increase in the Ps arrival time corresponds to a depth increase of up to 30 km (using the IASP91 model), as indicated by the gray bars in the RF cross-sections of Fig. 3.

The Ps-P travel time differences (Fig. 4a and b) were converted to depth using an IASP91 model corrected by the upper mantle model SL2013sv (Schaeffer and Lebedev, 2013). For each 3° x 3° window an SL2013sv average 1D model was obtained, and the vertical S-wave travel time was compared to IASP91. The % deviation of this 1D model was used to update the IASP91 P and S velocities used later to convert Ps-P times to depth. This means that the time to depth conversion uses the same average Vp/Vs of the IASP91 model.

A 600 km wide Gaussian smoothing was applied to the gridded depths to reduce noise in the RF traces and enhance the main regional features. Fig. 4c and d shows the resulting depths of the 410 and 660 discontinuities. The maps of picked times (Fig. 4a and b) show early times near cratonic regions such as the São Francisco craton, the Amazon craton (Central Brazil Shield and the Amazon Basin) and the cratonic nucleus beneath the Parnaíba Basin due to high velocities in the upper mantle. Interestingly, after conversion to depth using the SL2013sv model, which takes into account the upper mantle fast velocities, no anomalous depth in those cratonic areas are seen in Fig. 4c and d.

3. Discussion

The 410 is reasonably stable in most of the continent (Fig. 4c), not differing much from the nominal 410 km depth. The 660 discontinuity, on the other hand, shows a wide region of deeper depth, south of 15°S (Fig. 4d, beneath the Pantanal, Chaco and southern Paraná basins). Fig. 5 shows the difference between the depths of the 410 and 660 discontinuities. The major feature observed in our continental-scale study is the deeper 660 km discontinuity. Fig. 5 shows a long region with thicker MTZ (green areas) roughly parallel to the subduction zone from Venezuela to Uruguay. North of about 15° S, this zone of deep 660 discontinuity is relatively narrow and centered around the expected slab location (between Benioff depths of 400 and 600 km), while south of 15°S it is much wider.

Several tomography studies have shown that in the central and northern part of South America, the Nazca slab plunges more steeply into the lower mantle, while in the southern part of the continent it remains stagnant for a long distance (Simmons et al., 2012; Fukao and Obayashi, 2013; Schaeffer and Lebedev, 2013; Scire et al., 2017; Melo et al., 2019; Portner et al., 2020; Rodríguez et al., 2021; Celli et al., 2020; Ciardelli et al., 2021). The average eastern limit of the
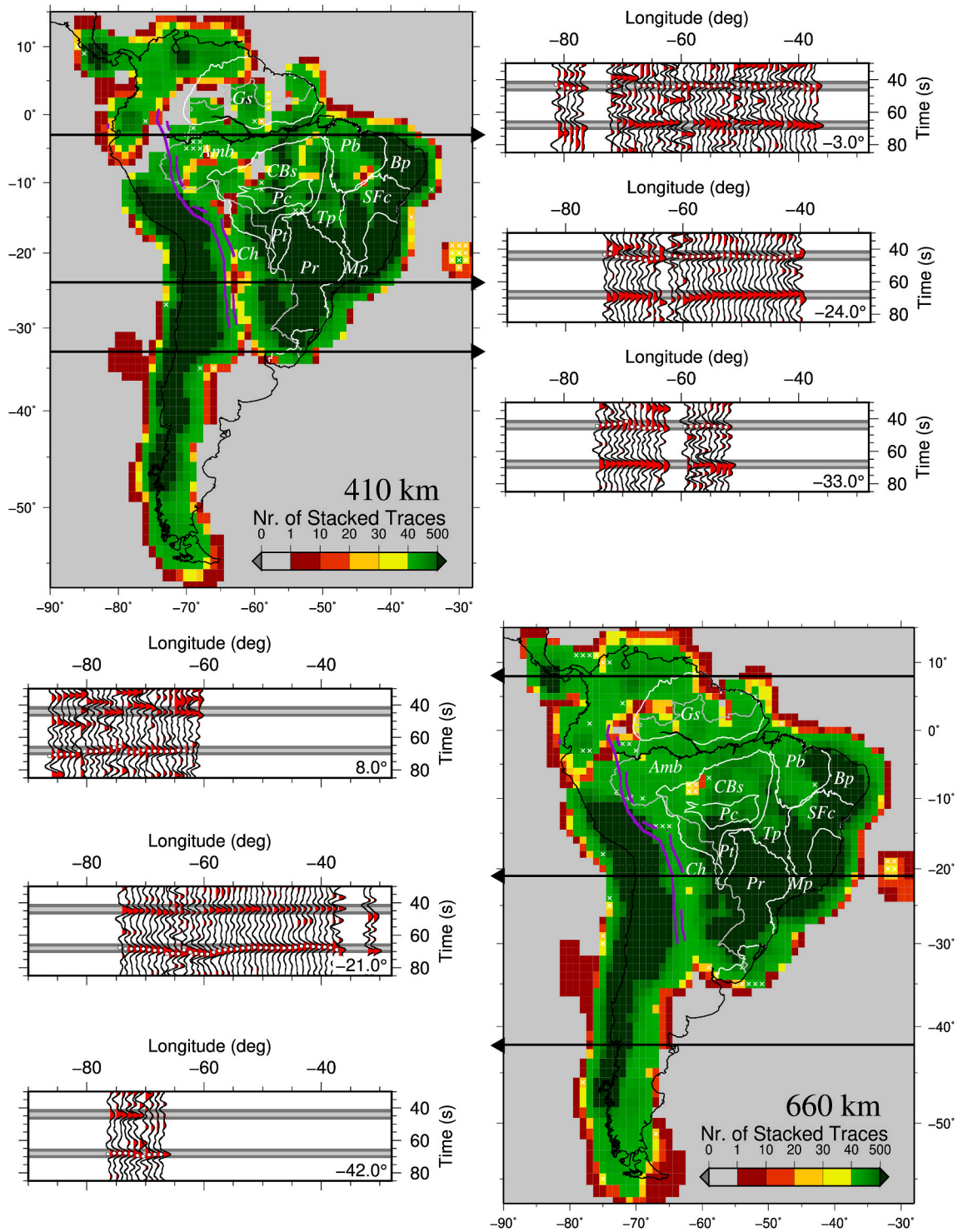
Fig. 3. Density map of piercing points, and examples of RF sections. The maps show the number of stacked piercing points for moving windows of 3°x 3° giving an ideia of the resolution of the dataset. Three sections of stacked RFs are shown for each discontinuity. In the RF sections the gray bars indicate a time difference corresponding to ±10 km (inner light gray) and ±30 km (outer dark gray) with respect to the nominal 410 and 660 km depths (IASP91 model). The peaks of the Ps conversions are marked by white circles. Note the increase of the Ps time of the 660 conversion in the two profiles in Central and southern South America (21°S and 42°S). The cells marked with a white "x" denote picks discarded because of very poor signal. The main geological provinces in the stable continent are: cratonic areas: Gs and CBs = Guyana and Central Brazil shields, SFc = São Francisco craton. Brasiliano foldbelt provinces: Bp = Borborema, Tp = Tocantins, Rb = Ribeira provinces. Intracratonic Paleozoic basins: Amb = Amazon, Pb = Parnaíba, Pc = Parecis, Pr = Paraná, Ch = Chaco basins. Pt = Quaternary Pantanal basin. The purple lines are the 400 and 600 km depth Benioff zone (Slab1.0 model).
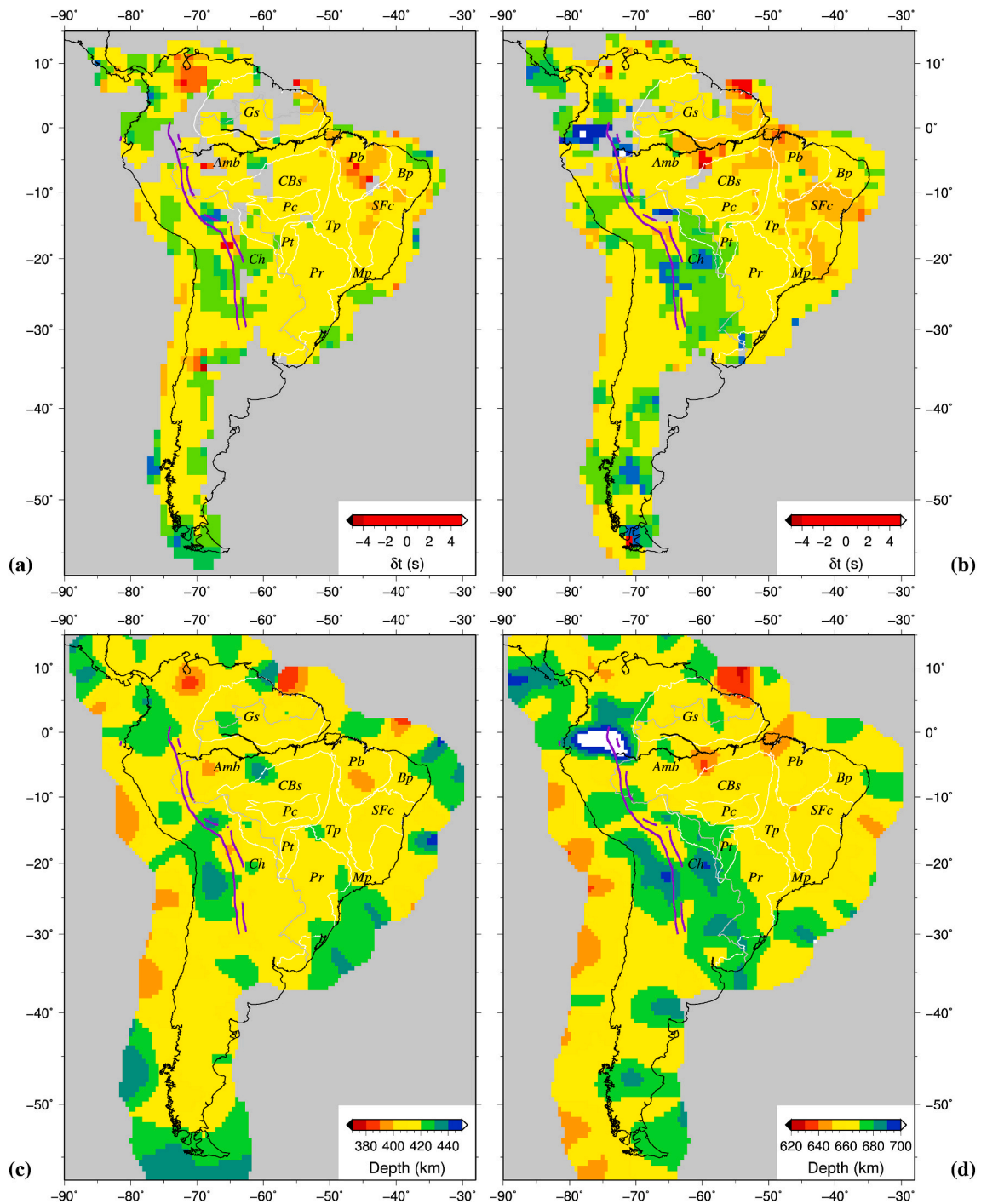
Fig. 4. Picked residual times with respect to IASP91 model (top row, a and b) and converted depths (bottom row, c and d) of the 410 and 660 km discontinuities. Depths were slightly smoothed to enhance the regional trends. The purple lines are the 400 and 600 km depth Benioff zone (Slab1.0). Province labels as in Fig. 3.

sub-horizontal slab, as imaged by those tomographic models, near 660 km depth is indicated by the solid black line in Fig. 5.

Instead of stacking RFs grouped by nearby piercing points (using 3°x3° wide cells), we also tested estimating the MTZ thickness by stacking all RFs from each station, shown in Fig. S5. This reduces the influence of velocity anomalies in the upper mantle, but the stacked RFs

are averages of a slightly wider area (up to ~440 km diameter for the 660 km). At any rate, the same pattern of thicker MTZ is seen between the 600 km Benioff zone and the east limit of the stagnant slab near 660 km (Fig. S5).

More detailed tomography inversions around the Pantanal Basin (Dragone and Bianchi., 2019; Ciardelli et al., 2021) suggest that the
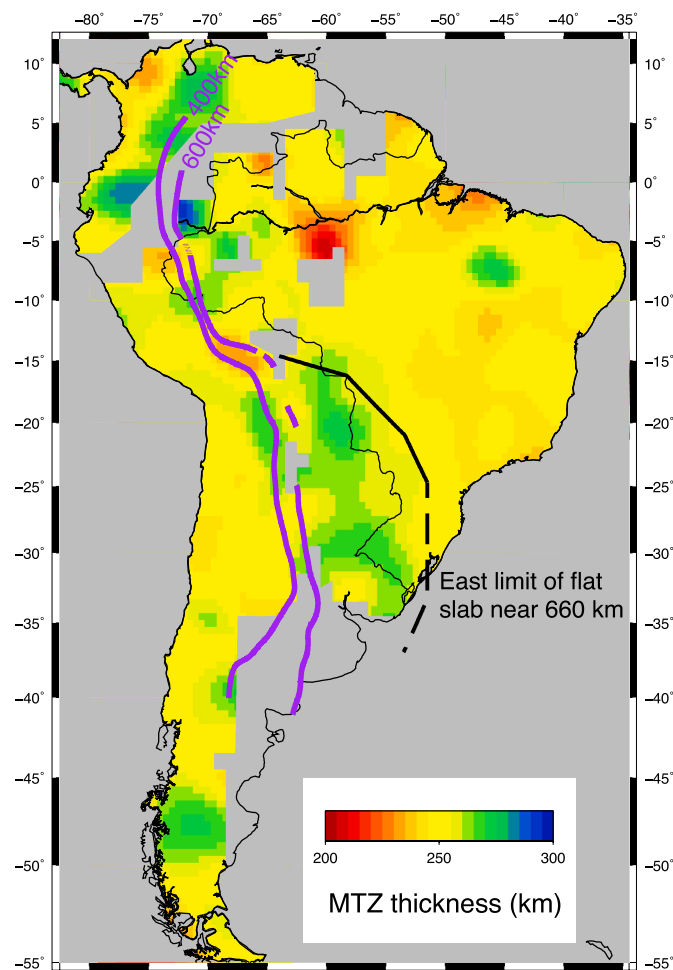
Fig. 5. Thickness of the mantle transition zone (i.e., difference between the depths of Fig. 4c and d). The solid black line is the Eastern limit of the stagnant Nazca slab near the 660 km depth, based on several tomography models (see text). Note the wide region of thick MTZ (green areas) south of 15°S. North of 15°S, the thicker MTZ seems to be closer to the more steeply dipping slab, but the resolution in that region is poor (See Fig.4 a,b). This different behavior is interpreted as due to the stagnant slab near the 660 discontinuity in the south, and a more steeply plunging slab to the north. The purple lines are the 400 and 600 km depth Benioff zone from Slab2 model (Hayes et al., 2018); north of 0° and south of 30°S, Slab2 used tomography models to estimate the slab depth.

Nazca slab is stagnant above the 660 discontinuity south of 25°S. Beneath the Pantanal Basin and north of 25°S, the slab drops below the MTZ. This means that over a large region (from about 35°S to 15°S) the cold Nazca slab is very close to 660 km depth, which would explain the extended region of deeper 660-km discontinuity seen in Fig. 5.

Fig. 6 shows two E-W profiles of stacked receiver function, one at 12°S across the Amazon craton to the north of the Pantanal basin, and another along 18°S across the Pantanal. The S velocities of the global SL2013sv model (Schaeffer and Lebedev, 2013) and the more regional SA2019 model of Celli et al. (2020) are also shown for comparison. In the Amazon craton, the Nazca slab is too deep to affect the 660 discontinuity, which remains at its nominal depth. Across the Pantanal, however, both the SL2013sv and SA2019 models show high velocities in the transition zone, which causes a deflection of the 660 discontinuity of 10–20 km from 65°W to 54°W (Figs. 5 and 6d).

The models SL2013sv and SA2019 do not have good resolution beneath the transition zone and are not able to discriminate between models with the stagnant slab inside the transition zone, such as the global models of Simmons et al. (2012) and Fukao and Obayashi (2013), from the more regional models of Portner et al. (2020) and Rodríguez

et al. (2021) which show the slab just beneath the transition zone. One explanation for this inconsistency may be that the stagnant Nazca slab is above the 660 discontinuity south of ~25°S but drops gradually below the transition zone from ~25°S to 15°S. North of the Pantanal Basin (Fig. 6a and b) the Nazca slab plunges directly into the lower mantle. This observation indicates a large region where the stagnant slab crosses the 660-km discontinuity. Interestingly, the inferred change of geometry of the Nazca Slab from stagnant, just beneath the MTZ in the south, to plunging into the lower mantle, in the north, occurs beneath the Quaternary Pantanal basin. Perhaps this slab geometry could induce a flow pattern in the upper mantle causing subsidence of the Pantanal region, which deserves further investigations.

The fact that we observe a lowering of the 660 but not a rise of the 410, could be explained by the fact that the stagnant slab remains close to the 660 km (just above in the South, and just below near the Pantanal) but never too close to the 410 discontinuity. Thus, we interpret the deeper depth of the 660 discontinuity as due to cooling effect of this stagnant Nazca slab, as shown in Figs. 5 and 6.

Other interesting features in Fig. 5 are the thicker transition zone beneath the Parnaíba basin in Northeastern Brazil, and the negative anomaly in the middle of the Amazon basin. In the Parnaíba basin (Coelho, 2019) did not detect any anomalous depths of the 410 and 660 km. As for the negative anomaly beneath the Amazon basin, it coincides with low velocities near 600 km depth in several models such as LLNL-G3Dv3 (Simmons et al., 2012), SAM5 (Rodríguez) and SA2019 (Celli et al., 2020) and SAAM23 (Ciardelli et al., 2021). However, both MTZ anomalies are due to small numbers of stacked RFs (Figs. 2 and 3) and will need more data to be confirmed.

Other interesting features in the RF profiles (Fig. 6) is the negative peak likely due to the lithosphere/asthenosphere boundary (LAB). Beneath the high velocity regions of the Amazon and S. Francisco cratons, the LAB is around 200 km deep. Beneath the Pantanal basin (Fig. 6d), characterized by low velocities at asthenospheric depths, the LAB rises to ~150 km. This indicates lithospheric thinning, as implied by the low velocities at 100–200 km depth from teleseismic tomography of P waves (Rocha et al., 2019; Portner et al., 2020) and S waves (Rodríguez et al., 2021). However, more detailed studies of this possible LAB negative peak in the stacked receiver functions are necessary to make sure it is not contaminated by crustal reverberations.

4. Conclusion

A large data set of receiver functions has been processed covering almost all the Andean range and large parts of the stable continental interior of South America (Fig. 1). Some areas still lack good coverage, such as Northern Peru, NW Amazon, the Guyanas and eastern Argentina (Fig. 2). However, the coverage in the central part of the continent was good enough to reveal a regional-scale depression of the 660 km discontinuity of up to 30 km, beneath the Chaco, Pantanal and southern Paraná basins (Figs. 5 and 6).

We interpret this depression of the 660 discontinuity as due to cooling effect of the stagnant Nazca slab. The laterally wider zone of discontinuity depression correlates well with the long stagnant geometry of the Nazca slab in the SE part of the continent, before it plunges again into the lower mantle near the SE Atlantic coast (Rodríguez et al., 2021). The fact that the 410 km discontinuity does not seem to be much affected may be an indication that the position of the stagnant, cold Nazca slab is close the 660 km depth (just above or just below the mantle transition zone), as revealed by the more recent regional tomography results.

Declaration of competing interest

The authors declare that they have no known competing financial interests or personal relationships that could have appeared to influence the work reported in this paper.
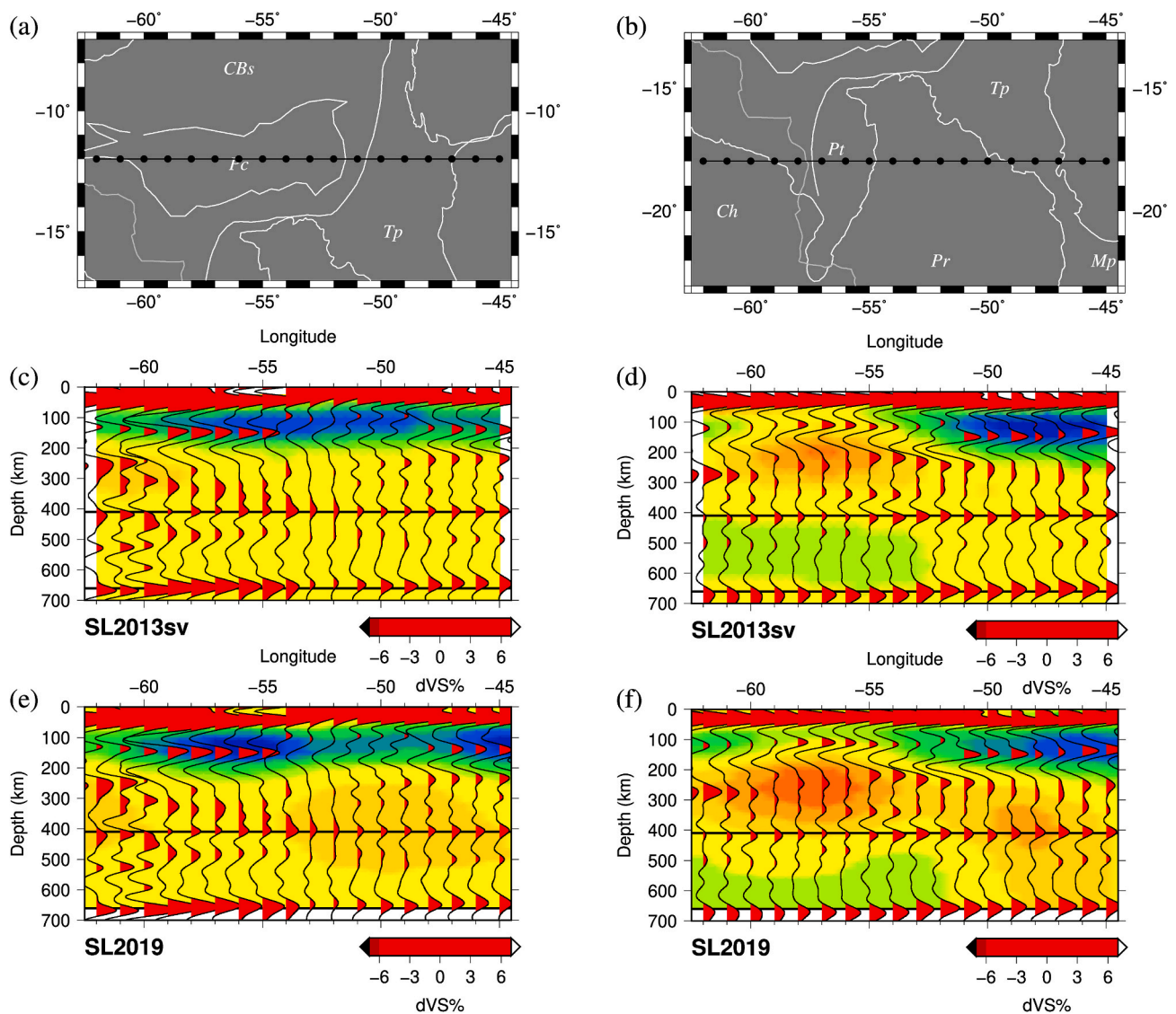
Fig. 6. RF cross sections compared with S-wave velocity anomalies (models SL2013Sv and SA2019). In the maps (top row) each dot corresponds to one stacked receiver function in the sections below. In the Amazon craton (left column, profile at 12°S), the cold slab is too deep to cause any effect on the 660-km discontinuity. Across the Pantanal (right column, profile at 18°S), on the other hand, the presence of the stagnant, cold slab makes the 660 discontinuity deeper by ∼10–30 km.

Acknowledgements

Appendix A. Supplementary data

Supplementary data to this article can be found online at https://doi.org/10.1016/j.jsames.2021.103607.

Author statement

Marcelo Bianchi: Conceptualization, Methodology, Formal analysis, Visualization, Writing Original draft and Review editing. **Marcelo Assumpção:** Formal analysis, Writing Original draft and Review editing, Funding aquisition. **Clinton Koch and Susan Beck:** Resources and Data Curation, Writing – review & editing.

References

Ballmer, M.D., Schmerr, N.C., Nakagawa, T., Ritsema, J., 2015. Compositional mantle layering revealed by slab stagnation at ∼1000-km depth. Sci. Adv. 1, e1500815, 2015.

Bianchi, M.B., Assumpção, M., Rocha, M.P., Carvalho, J.M., Azevedo, P.A., Fontes, S.L., Dias, F.L., Ferreira, J.M., Nascimento, A.F., Ferreira, M.V., Costa, I.S.L., 2018. The Brazilian seismographic network (RSBR): improving seismic monitoring in Brazil. Seismol Res. Lett. 89 (2A), 452–457. https://doi.org/10.1785/0220170227.

Bina, C.R., Helffrich, G., 2014. Geophysical constraints on mantle composition In: Treatise on Geochemistry, second ed., vol. 3. Elsevier Inc., pp. 41–65

Coelho, D.L.O., 2019. Passive Source Seismology in the Parnaíba Basin: Implications for Cratonic Subsidence. Ph.D. Thesis (part in Portuguese, part in English). Federal University of Rio Grande do Norte, Geodynamics and Geophysics Program, p. 150pp. https://repositorio.ufrn.br/handle/123456789/28621.

Braunmiller, J., Lee, S.V.D., Doermann, L., 2006. Mantle transition zone thickness in the central South-American subduction zone. In: Earth's Deep Water Cycle. American Geophysical Union (AGU), pp. 215–224. doi:10.1029/168GM16.

Celli, N.L., Lebedev, S., Schaeffer, A.J., Ravenna, M., Gaina, C., 2020. The upper mantle beneath the South Atlantic Ocean, South America and Africa from waveform tomography with massive data sets. Geophys. J. Int. 221 (1), 178–204.

Ciardelli, C., Bozdag, E., Assumpção, M., van der Lee, S., 2021. Adjoint Tomography of South America and Geometry of the Nazca Slab. Seismol. Soc. Am. Annual Meeting, Abstract.

Dragone, I.A., Bianchi, M.B., 2019. P-wave tomography sensibility test applied to the Chaco-Paraná, Paraná and Pantanal basins inversion. Third Brazilian Seismology Symposium, Vinhedo, SP, Brazil, pp. 15–17. April 2019, Abstract.

Feng, M., Van der Lee, S., Assumpção, M., 2007. Upper mantle structure of South America from joint inversion of waveforms and fundamental-mode group velocities of Rayleigh waves. J. Geophys. Res. 112, B04312. https://doi.org/10.1029/2006JB004449.

Fukao, Y., Obayashi, M., 2013. Subducted slabs stagnant above, penetrating through, and trapped below the 660 km discontinuity. J. Geophys. Res.: Solid Earth 118 (11), 5920–5938.

Gilbert, H.J., Sheehan, A.F., Wiens, D.A., Kennet, G.D., Dorma, L.M., Hildebrand, J., Webb, S., 2001. Upper mantle discontinuity structure in the region of the Tonga Subduction Zone. Geophys. Res. Lett. 28 (9), 1855–1858.

Hayes, G.P., Wald, D.J., Johnson, R.L., 2012. Slab1.0: a three-dimensional model of global subduction zone geometries. J. Geophys. Res.: Solid Earth 117 (B1).

Hayes, G.P., Moore, G.L., Portner, D.E., Hearne, M., Flamme, H., Furtney, M., Smoczyk, G.M., 2018. Slab2, a comprehensive subduction zone geometry model. Science 362 (6410), 58–61.

Hosseini, K., Sigloch, K., Tsekhmistrenko, M., Zaheri, A., Nissen-Meyer, T., Igel, H., 2020. Global mantle structure from multifrequency tomography using P, PP and P-diffracted waves. Geophys. J. Int. 220, 96–141. https://doi.org/10.1093/gji/ggz394. URL:

Huang, Q., Schmerr, N., Waszek, L., Beghein, C., 2019. Constraints on seismic anisotropy in the mantle transition zone from long-period SS precursors. J. Geophys. Res.: Solid Earth 124, 6779–6800. https://doi.org/10.1029/2019JB017307.

Lawrence, J.F., Shearer, P.M., 2006. A global study of transition zone thickness using receiver functions. J. Geophys. Res. 111, B06307. https://doi.org/10.1029/2005JB003973.

Li, X., Kind, R., Yuan, X., 2003. Seismic study of upper mantle and transition zone beneath hotspots. Phys. Earth Planet. In. 136, 79–92.

Litasov, K.D., Ohtani, E., Sano, A., 2006. Influence of water on major phase transitions in the Earth`s mantle. Geophys. Monogr. Am. Geophys. Union 168, 95–111.

Liu, K.H., Gao, S.S., Silver, P.G., Zhang, Y., 2003. Mantle layering cross central South America. J. Geophys. Res. 108 (B11), 2510. https://doi.org/10.1029/2002JB002208.

Melo, B.C., Celli, N.L., Lebedev, S., de Laat, J., Assumpção, M., 2019. Towards High-Resolution Waveform Tomography of South America. AGU Fall Meeting, 2019, Abstract.

Pinheiro, A.G., Julià, J., 2014. Normal thickness of the upper mantle transition zone in NE Brazil does not favor mantle plumes as origin for intraplate Cenozoic volcanism. Geophys. J. Int. 199 (2), 996–1005. https://doi.org/10.1093/gji/ggu281.

Petersen, N., Vinnik, L., Kosarev, G., Kind, R., Oreshin, S., Stammler, K., 1993. Sharpness of the mantle discontinuities. Geophys. Res. Lett. 20 (9), 859–862.

Portner, D.E., Rodríguez, E.E., Beck, S., Zandt, G., Scire, A., Rocha, M.P., Bianchi, M.B., Ruiz, M., Sand França, G., Condori, C., Alvarado, P., 2020. Detailed structure of the subducted Nazca slab into the lower mantle derived from continent-scale teleseismic P-wave tomography. J. Geophys. Res.: Solid Earth e53955.

Rivadeneyra, C., Bianchi, M., Assumpção, M., Cedraz, V., Julià, J., Rodríguez, M., Sánchez, L., et al., 2019. An updated crustal thickness map of central South America based on receiver function measurements in the region of the Chaco, Pantanal, and Paraná Basins, southwestern Brazil. J. Geophys. Res. 124 https://doi.org/10.1029/2018JB016811.

Rocha, M.P., Assumpção, M., Affonso, G.M.P.C., Azevedo, P.A., Bianchi, M., 2019. Teleseismic P-wave tomography beneath the Pantanal, Paraná and Chaco-Paraná basins, SE south America: delimiting lithospheric blocks of the SW Gondwana assemblage. J. Geophys. Res. 124 https://doi.org/10.1029/2018jb016807.

Rodríguez, E.E., Portner, D.E., Beck, S.L., Rocha, M.P., Bianchi, M.B., Assumpção, M., Ruiz, M., Alvarado, P., Condori, C., Lynner, C., 2021. Mantle dynamics of the Andean Subduction Zone from continent-scale teleseismic S-wave tomography. Geophys. J. Int. 224 (3), 1553–1571. https://doi.org/10.1093/gji/ggaa536.

Schaeffer, A.J., Lebedev, S., 2013. Global shear speed structure of the upper mantle and transition zone. Geophys. J. Int. 194, 417–449. https://doi.org/10.1093/gji/ggt095.

Schmerr, N., Garnero, E.J., 2007. Upper mantle discontinuity topography from thermal and chemical heterogeneity. Science 318 (5850), 623–626. https://doi.org/10.1126/science.1145962.

Scire, A., Zandt, G., Beck, S., Long, M., Wagner, L., 2017. The deforming Nazca slab in the mantle transition zone and lower mantle: constraints from teleseismic tomography on the deeply subducted slab between 6° S and 32° S. Geosphere 13 (3), 665–680.

Shearer, P.M., Masters, G., 1992. Global mapping of topography on the 660-km discontinuity. Nature 355, 791–796.

Simmons, N.A., Myers, S.C., Johannesson, G., Matzel, E., 2012. LLNL-G3Dv3: global P wave tomography model for improved regional and teleseismic travel time prediction. J. Geophys. Res. 117, B10302. https://doi.org/10.1029/2012JB009525, 2.

Smyth, J.R., Jacobsen, S.D., 2006. Nominally anhydrous minerals and Earth's deep water cycle. AGU Geophys. Monogr. Ser. 168, 1–11.

VanDecar, J.C., James, D.E., Assumpção, M., 1995. Seismic evidence for a fossil mantle plume beneath South America and implications for plate driving forces. Nature 378, 25–31.

Wood, B.J., 1995. The effect of H20 on the 410-kilometer seismic discontinuity. Science 268, 74–76.

Update

Journal of South American Earth Sciences

Corrigendum to "Effect of the Cold Nazca Slab on the Depth of the 660 km Discontinuity in South America" [J. S. Am. Earth Sci. (2021) 112, 103607]

Marcelo Belentani Bianchi [a], Marcelo Assumpção [a,*], Clinton Koch [b], Susan Beck [b]

[a] University of São Paulo, Institute of Astronomy, Geophysics and Atmospheric Sciences, Brazil
[b] University of Arizona, Department of Geosciences, USA

The authors regret that Figures 4 a,b and Fig. 6 c,d,e,f came out with a problem in the color scale bar. The correct figures are shown below.

The authors would like to apologise for any inconvenience caused.